

1 Squirt flow due to interfacial water films in hydrate bearing sediments

2

3 Kathleen Sell¹, Beatriz Quintal², Michael Kersten¹ and Erik H. Saenger^{3,4}

4

5 ¹Johannes Gutenberg-University Mainz, Germany

6 ²University of Lausanne, Switzerland

7 ³ International Geothermal Centre, University of Applied Sciences Bochum, Germany

8 ⁴ Ruhr University Bochum, Germany

9

10 Correspondence to: Kathleen Sell (sell@uni-mainz.de)

11

12 *Please note: All our responses to remarks of reviewers are in red and italic.*

13

14 *Dear Anonymous Reviewers,*

15 *We appreciate the time, interest and effort you invested to evaluate our manuscript. In the*
16 *following, we respond to your questions, comments and concerns in order of appearance, to*
17 *improve our manuscript based on your valued input.*

18 *Kind Regards,*

19 *Kathleen Sell, Beatriz Quintal, Michael Kersten, and Erik H. Saenger*

20

21

22 Anonymous Referee #1

23 Received and published: 23 October 2017

24 Review type: Interactive comment

25 <https://doi.org/10.5194/se-2017-106>, 2017

26

27 The paper presents a model study on absorption based on a squirt flow model in hydrate-bearing
28 sediments. The setup of the model is straight forward and based on visual observations of thin
29 (sub-micron) water films between quartz sand grains and clathrate. The mechanism which
30 creates a pressure gradient and following flow in the water film is described clearly and also
31 the influences of different water film thickness, different grain sizes, presence of isolated water
32 pockets in the hydrate and, the influence of connections between the water films. The shift of
33 the maximum in the dependence of $1/Q$ on frequency with changing thickness of the water film
34 shows, that a distribution of various film thicknesses would result in high absorption ($1/Q$) over
35 a broad frequency range. This is what one would expect, because the high absorption of hydrate-

36 bearing sediments has been observed in the field at seismic frequencies and in the lab at
37 ultrasonic frequencies. The paper provides a valuable contribution towards the understanding
38 of possible absorption mechanisms in hydrate-bearing sediments and should be published soon.

39 However, to avoid the “misuse” of the model in the interpretation of real measurements the
40 author should clearly state what the restrictions and limits of the model are. The visual
41 observations used for the modelling should also be brought in relation to other visual observations
42 (see comment/reference below). The following two main restrictions, at least, should be pointed
43 out to the reader:

44 The model is based on the observations/results from high-resolution synchrotron-based X-ray
45 micro-tomography, where the hydrate is produced with the “gas in excess method”. The
46 method used for the hydrate formation is essential to understand the resulting hydrate habit.
47 The “gas in excess method” forms a grain coating hydrate structure (with a water film between
48 hydrate and grains), because the water which is wetting the grains is transformed into hydrate.
49 When hydrate is formed with the “water in excess method” the grains will also be water wet,
50 but these very thin (sub-micron) hydrate films between the grains and the hydrate structure will
51 only occur at very high hydrate saturations (the highest reported values to my knowledge are
52 about 90% from Mallik and the Gulf of Mexico).

53 *Authors: As suggested by the reviewer we added the mandatory information in the Introduction*
54 *as well as in section 2.*

55 See also Tohidi’s paper: “Gas bubbles, when present, act as preferential nucleation sites, but
56 silica glass surfaces are wetted strongly by water and do not promote heterogeneous surface
57 nucleation; a surface water film remains to high clathrate saturations. The fact that hydrates
58 grow within the center of pores, rather than on grain surfaces, is likely to restrict the potential
59 for cementation of sediments, unless a large proportion of the pore space is filled with hydrate.”

60 Tohidi, B., Anderson, R., Clennell, M. B., Burgass, R. W., & Biderkab, A. B. (2001). Visual
61 observation of gas-hydrate formation and dissociation in synthetic porous media by means of
62 glass micromodels. *Geology*, 29(9), 867-870.1)

63 This model with sub-micron bound-water films is restricted to very high hydrate saturations
64 (for your model with 250 – 150 m grain size and a water film below 1µm calculated about 99%
65 hydrate saturation) or to gas-bearing reservoirs where the free water, available for hydrate
66 formation, has been completely transformed into hydrate.

67 *Authors: Indeed, the information that for our type of model the assumed GH saturation will be*
68 *very high <90% was missing. Therefore, this fact has been added to the Introduction section.*

69 The model (e.g. Fig. 7 & Fig. 12) assumes the sand grain as an inclusion in the hydrate matrix
70 (a suspension of quartz grains in hydrate). This neglects the fact that hydrate is a secondary
71 phase forming in the pore space when the sediment already has deposited and forms a grain
72 skeleton with grain-to-grain contacts. Depending on the number and size of these contacts
73 (compaction, overburden) the modulus (mainly the real part of the complex modulus) of the
74 hydrate free grain skeleton will vary. Q is derived from the ratio of imaginary part and the real
75 part of the complex modulus and will, therefore, change when the real part changes due to
76 different number of grain-to-grain contact (coordination number). 2) The specific properties of
77 the sediment grain skeleton and the resulting influence on absorption are not considered.

78 *Authors: It is true that our model is a very simplified approach regarding sedimentary systems*
79 *with respect to grain contacts and therefore a first step towards more realistic matrices as*
80 *stated in the conclusion part. We are aiming for SRXCT/HRXCT data input to extend our model*
81 *approach. But for now we are limited to the simple scenario of unconsolidated sediments.*

82 *We added your valuable comment to our Results section.*

83 To study this special squirt-flow mechanism related to the existence of thin water films initially
84 separated from other influences is certainly justified. However, this model can be improved in
85 future to also involve effects from the grain skeleton (e.g. involving Hertz-Mindlin theory) and
86 it can be combined with other absorption mechanisms (see Marin-Moreno's paper).

87 *Authors: Further investigations involve the stepwise extension of this model towards more*
88 *realistic settings is aimed but hampered by the lack of a segmentation routine capable to cover*
89 *a full dataset (24GB). Currently a machine learning code is tested on the data to handle this*
90 *issue.*

91

92

93 Anonymous Referee #2

94 Received and published: 20 November 2017

95 Review type: Interactive comment

96

97 <https://doi.org/10.5194/se-2017-106>, 2017

98

99 Dear authors,

100 I found your paper intriguing and comprehensive; in my understanding, you provide previously
101 published observational evidence from x-ray tomography to support the claim that a thin water
102 film around sand grains embedded in a gas hydrate matrix is a good conceptual model that
103 captures the high attenuation observed in gas hydrate systems. I believe that the general scope
104 of your paper deserves some attention as squirt flow in hydrates is only recently being
105 considered as the responsible mechanism and Marin-Moreno et al. (2017) is potentially too
106 confusing for scientists to use as it considers the overlap of many mechanisms. So there is
107 definitely a gap in the literature for simple, usable models of the squirt flow of GH and I think
108 your paper is a step towards the right direction. I do however think that the presentation of your
109 work does not do the ideas justice and as a result lessens the potential significance it may have.
110 Below are some of my most serious concerns:

111 1. I am not entirely familiar with imaging techniques when applied to hydrates so I am not
112 aware how the conceptualisation of your model is affected by the imaging. I realise the
113 experimental imaging results are presented elsewhere but I would still like to see a convincing
114 argument about how the thin water film surrounding a quartz grain within a hydrate is indeed a
115 physically plausible configuration rather than an imaging artifact

116 *Authors: A common image artifact occurring when conducting synchrotron-based tomography*
117 *is the so-called edge enhancement. Probably, this is the artifact you have in mind. When plotting*
118 *a histogram over an area where possible edge enhancement occurs the histogram line plot will*
119 *reveal symmetrical valleys and peaks. Here, this is not the case because we can identify a*
120 *several voxel wide interface between the GH and quartz. This interface is in the same gray-*
121 *value range than the water phase identified in the initial (untreated) samples – these samples*
122 *are completely GH free and we can be sure that the phase identified is water. The observation*
123 *of the interfacial water layer from the experimental results of Chaouachi et al. (2015) is in*
124 *accordance with the publication of Tohidi et al. (2001). Additionally several molecular*
125 *numerical simulations showed that a water layer prefers the interface of GH and quartz grains*
126 *(Bagherzadeh et al., 2012; Bai et al., 2011; Liang et al., 2011). For the matter of clarification*
127 *text passages have been added to the manuscript.*

128 2. Your single circular grain model presented in Figure 7 is the exact same model proposed by
129 White, J. (1975) which you cite in passing in your introduction. The only difference here is that
130 your sand grain is in place of a second fluid in White's model. This is nowhere mentioned and
131 I firmly believe it should be.

132 *Authors: Our model might, in principle, resemble White's model from the spherical geometries*
133 *involved, but it is considerably different. White's model refers to a spherical porous patch*
134 *embedded in a porous background. Fluid pressure diffusion occurs between those two*
135 *poroelastic subdomains across the spherical surface. The model that we consider refers to a*
136 *non-porous solid spherical inclusion separated from the embedding non-porous solid*
137 *background by a thin liquid shell. In this case, fluid pressure diffusion occurs only within the*
138 *liquid shell, tangentially to its spherical surfaces.*

139 3. You claim to numerically solve (1), (2) but you show no meshing and mention no restrictions
140 on your domains (is the circular sand grain obeying a free BC, is it fixed etc?)

141 *Authors: We have added a figure with a mesh for the main model (new Figure 8) and all the*
142 *necessary BC are explained in the Numerical Methodology section.*

143 4. As I mentioned earlier in comment 2 this model is exactly the same as White's model which
144 has an exact analytic solution. Why does your model of figures 7,14 not have an analytic
145 solution despite the simple domain and, if it does, why are we not seeing it - it is so much easier
146 for someone to replicate your work if they have a formula to use. Does your model agree with
147 White's model if his second fluid becomes really stiff (to the limit of a sand grain)?

148 *Authors: Our model is different than White's model, as explained above. We believe this is*
149 *clearer after our revision.*

150 5. Although these may be commonplace for people familiar with squirt flow, how do you define
151 "mesoscopic" as a scale here? What are the domains and boundary conditions that go into
152 solving your equations? How does the relative rather than absolute scaling affect the behaviour
153 of your attenuation curves? What I mean here is that if you fixed the GH square in model 7 to
154 have side = 1 you could see the affect of relative saturation of GH and water rather than inserting
155 absolute values. This would be much more illuminating than your figure 8. This problem is also
156 present when you discuss water bridges and your model demonstrates a second peak in the
157 attenuation curves but the reader is left wondering how(if?) does this peak move when the
158 bridge gets longer. There is significant mathematical rigour that is missing from your work

159 which is not in itself always a bad thing but this impedes the impact and significance it may
160 have.

161 *Authors: Our model is not at the mesoscopic scale, but microscopic. With respect to*
162 *mathematical rigor, we believe that we gave the necessary information, such as the equations,*
163 *the parameter values, the model geometry, and the boundary conditions are described in the*
164 *numerical methodology part.*

165 6. You mention shear dispersion in passing indicating that you have numerically calculated it
166 ("it can be calculated in a similar manner simply by changing the boundary conditions") - is the
167 shear dispersion predicted by this model in any way realistic? I feel that it would be beneficial
168 for your work to show the attenuation and dispersion of shear velocity and discuss the
169 success/limitation of your modelling strategy with respect to shear.

170 *Authors: Unfortunately our code becomes unstable under the boundary condition necessary for*
171 *a shear test and the results for S-wave attenuation and dispersion at this point are not reliable.*
172 *The compressional tests to obtain P-wave attenuation and dispersion, on the other hand, have*
173 *been tested through comparisons with other solutions (e.g., Quintal et al, 2016, Geophysics)*
174 *and yield stable and reliable results.*

175

176 And some more minor comments:

177 - Figure 2 have some labels GH* and I have not been able to see what the * refers

178 - Figure 3 caption has an unrendered mu character that shows up as a box

179 - P20L5 needs a space between "effect" and "of"

180 *Authors: These mistakes have been fixed.*

181

182

183

184

1 Squirt flow due to interfacial water films in hydrate bearing 2 sediments

3 Kathleen Sell^{1†}, Beatriz Quintal², Michael Kersten¹, and Erik H. Saenger^{3,4}

4

5 ¹ Johannes Gutenberg-University Mainz, Germany

6 ² University of Lausanne, Switzerland

7 ³ International Geothermal Center, [Bochum](#) University of Applied Sciences [Bochum](#), Germany

8 ⁴ Ruhr University Bochum, Germany

9

10 † Corresponding author (sell@uni-mainz.de)

11

12 ABSTRACT

13 Sediments containing gas hydrate dispersed in the pore space are known to show a
14 characteristic seismic anomaly which is a high attenuation along with increasing seismic
15 velocities. Currently, this observation cannot be fully explained albeit squirt-flow type
16 mechanisms at-on the microscale have been speculated to be the cause. Recent major findings
17 from in-situ experiments, using the gas in excess and water in excess formation method, and
18 coupled with high-resolution synchrotron-based X-ray micro-tomography, revealed a
19 systematic presence of thin water films between the quartz grains and the encrusting hydrate
20 when formed using the “gas in excess method”. ~~In this study, †~~The data ~~was~~ obtained from
21 ~~those~~ experiments ~~and underwent here submitted~~underwent ~~to~~ an image processing
22 procedure to quantify the thicknesses and geometries of the aforementioned interfacial water
23 films. Overall, the water films vary from sub- μm to a few μm in thickness. ~~where and s~~
24 addition, some of them the water films are interconnected byinterconnect through
25 water bridges. This geometrical analysis is ~~then~~ used to propose a new conceptual squirt flow model
26 for hydrate bearing sediments. A series of numerical simulations is performed considering
27 variations of the proposed ~~Subsequently the established model acts as a direct model input to~~
28 ~~obtain~~to study seismic attenuation caused by such thin water films. Our results support previous
29 speculations that squirt flow can explain high attenuation at seismic frequencies in hydrate
30 bearing sediments, but based on a conceptual squirt flow model which is geometrically
31 different than those previously considered.

32 Keywords: attenuation, squirt flow, interfacial films, dispersion, micro-tomography, gas
33 hydrates, sediments, numerical modeling

34

35

36

1

2 1. INTRODUCTION

3 Important mechanisms of wave attenuation in fluid-saturated porous media from seismic to
4 ultrasonic frequencies, include friction between grain boundaries (Winkler and Nur, 1982),
5 global flow or Biot's mechanism (Biot, 1962), and wave-induced fluid flow at mesoscopic and
6 microscopic scales (e.g., Müller et al., 2010). At the mesoscopic scale, patchy saturation and
7 fractures are the most prominent causes of wave-induced fluid flow (White, 1975; White et al.,
8 1975; Brajanovski et al., 2005; Tisato and Quintal, 2013; Quintal et al., 2014). At the
9 microscopic scale, wave-induced fluid flow is commonly referred to as squirt flow and
10 typically occurs between interconnected microcracks or between grain contacts and stiffer
11 pores (O'Connell and Budiansky, 1977; Murphy et al., 1986; Mavko and Jizba, 1991; Sams et
12 al., 1997; Adelinet et al., 2010; Gurevich et al., 2010). The attenuation caused by global flow
13 as well as that caused by wave-induced fluid flow at microscopic or mesoscopic scales are
14 frequency dependent. ~~W~~but while the latter can have a strong effect at seismic frequencies
15 (Pimienta et al., 2015; Subramaniyan et al., 2015; Chapman et al., 2016), global flow will only
16 cause significant attenuation in reservoir rocks at ultrasonic frequencies or higher (e.g., Bourbie
17 et al., 1987). The attenuation caused by friction between grain boundaries is, on the other hand,
18 frequency independent and basically depends on the confining pressure and the strain imposed
19 by the propagating wave (Winkler and Nur, 1982). Its effect is expected to be small for the
20 correspondingly small strains caused by seismic waves used in exploration and reservoir
21 geophysics. Furthermore, the attenuation caused by wave-induced fluid flow tends to be
22 linearly superposed to that due to friction between grain boundaries, as shown by Tisato and
23 Quintal (2014).

24 Gas hydrates (GH) are ice-like structures comprised of gas molecules entrapped by water
25 molecules (Sloan and Koh, 2008). The widespread global occurrence of GH and the fact that 1
26 m³ of GH contains up to 164 m³ of natural gas (CH₄ and CO₂ at standard conditions) draws
27 attention to the idea of using GH as a potential future energy resource (Schicks et al., 2011).
28 Nevertheless, GH-bearing sediments have been discussed not only as a relatively clean
29 hydrocarbon reservoir (Collett and Ladd, 2000), but also in terms of a geohazard that can
30 potentially contribute to global warming associated to hydrate dissociation and subsequent
31 destabilization of GH-cemented deep sea sediments at continental margins (Kvenvolden, 1993;
32 Nixon and Grozic, 2007). Occurrences of GH are restricted to locations providing the required
33 amount of gas and water and the preferred pressure-temperature (p/T) conditions, which are
34 commonly referred to as the so-called gas hydrate stability zones. Usually, GH reservoirs are
35 mainly limited to marine continental margins, deep lakes and permafrost regions (Bohrmann
36 and Torres, 2006).

37 In the search for GH reservoirs, the attenuation of seismic waves caused by the pore fluids
38 might be an important survey tool (e.g. Bellefleur et al. 2007). However, little effort has been
39 directed toward studying its effects for unconsolidated sediments hosting GH in a rather
40 dispersed manner. GH forming in the pore space of unconsolidated sediments at given p/T-
41 conditions alters the effective elastic and effective transport properties of the hosting sediment.
42 It is known that the presence of GH in the sediment not only reduces the porosity and causes

1 significant changes on its permeability, but also results in higher P- and S-wave velocities due
2 to stiffening of the hosting matrix (Dvorkin et al., 2003; Guerin & Goldberg, 2005; Yun et al.,
3 2005; Priest et al., 2006; Waite et al., 2009). In other words, the bulk and shear moduli increase
4 due to the GH matrix-supporting effect within the sedimentary frame (Ecker et al., 1998).
5 Additionally, the presence of GH causes higher attenuation of the seismic waves (Bellefleur et
6 al. 2007; Dewangan et al. 2014) which was in particular observed for sediments containing
7 dispersed GH in the pore space (Guerin and Goldberg, 2002; Dvorkin and Uden, 2004). This
8 ~~identified~~ anomalous seismic behavior in terms of increased attenuation and velocities (Guerin
9 and Goldberg, 2002; Dvorkin and Uden, 2004) cannot be fully explained, although wave-
10 induced fluid flow at the microscopic and mesoscopic scales have ~~has~~ been speculated to cause
11 them (Priest et al., 2006; Gerner et al. 2007). Gerner et al. (2007) conducted numerical P-wave
12 velocity simulations in highly permeable sedimentary layers, similar to hydrate-bearing
13 sediments, and identified interlayer flow at the mesoscopic scale (White et al., 1975) as a
14 potential mechanism of attenuation. Other authors have considered classical squirt flow models
15 (O'Connell and Budiansky, 1977; Murphy et al., 1986) as the main source of attenuation in
16 hydrate-bearing sediments (Dvorkin and Uden, 2004; Guerin & Goldberg, 2005; Priest et al.,
17 2006; Waite et al., 2009; Marin-Moreno et al., 2017).

18 Quantifying GH saturation levels through geophysical exploration techniques is, however, not
19 straightforward as there are still open questions on GH formation, its microstructure and
20 distribution in the natural settings. Additionally, the recovery of unaltered natural GH samples
21 is hampered due to their fast decomposition under ambient conditions. Therefore, various
22 researchers have attempted to mimic the natural environment of GH-bearing sedimentary
23 matrices in laboratory experiments (Berge et al., 1999; Ecker et al., 2000; Dvorkin et al., 2003;
24 Yun et al., 2005; Spangenberg and Kulenkampff, 2006; Priest et al., 2006, 2009; Best et al.,
25 2010, 2013; Hu et al., 2010; Li et al., 2011; Zhang et al., 2011; Dai et al., 2012; Schicks et al.,
26 2013). The results of this collective effort established a number of conceptual models for the
27 role of GH embedded in its sedimentary matrix (Figure 1). Nevertheless, these approximations
28 turned out to be still not satisfactory. Although it has been suggested that all hydrate habits
29 known from laboratory investigation involving synthetic samples occur also in nature
30 (Spangenberg et al. 2015), none of those simplified models can yield accurate predictions of
31 GH saturations from field electric resistivity or seismic data alone (Waite et al., 2009; Dai et
32 al., 2012).

33 Chaouachi et al. (2015) performed in-situ experiments based on the gas in excess method
34 different formation mechanisms, including the “gas in excess water in excess” and the “gas in
35 excess” method, to form gas hydrates in various sedimentary matrices. The in-situ
36 experiments are decoupled-coupled with high-resolution synchrotron-based X-ray micro-
37 tomography (SRXCT) yielded in 3D images of sub-µm spatial resolution for quartz sands
38 bearing GH. Using the “gas in excess” In this study, we introduce an alternative conceptual
39 model for GH formed with the “gas in excess method”. Using this formation method, the water
40 present in the samples weds the grain surfaces, and transforms into GH at the required
41 pressure/temperature conditions. When hydrate is formed with the “water in excess method”
42 the grains will also be water wet, but these very thin (sub-micron) hydrate films between the
43 grains and the hydrate structure will only occur at very high GH saturations. Furthermore, the

GH appears to form a rather coating structure surrounding the grain. Our study's objective bases based on findings from in-situ experiments coupled with high-resolution synchrotron-based X-ray micro-tomography (Chaouachi et al., 2015; Sell et al., 2016). The resulting 3D micro-tomography data for quartz sands bearing GH revealed the systematic presence of thin interfacial water films, between the pore-filling GH and the grains, independently of which formation method was used (gas in excess or water in excess method). The observed interfacial water films are occasionally interconnected via water bridges but also, as well as water pockets are embedded in the GH.

Here we submit For this study, the 3D-micro-tomography SRXCT data presented by Chaouachi et al. (2015) underwent to an image processing workflow in order to quantify the thicknesses of the thin interfacial water films. Based on the obtained results, we introduce a conceptual model for GH-bearing sediments to numerically study squirt flow. We perform numerical simulations of squirt flow in the proposed conceptual model to study the related allow for the dispersion of the stiffness-P-wave modulus and the corresponding frequency-dependent P-wave attenuation. The results demonstrate the high levels of seismic attenuation/dispersion that such features a range of variations of our conceptual model can cause. Additionally, our results and support the suggestions that the estimation of GH saturation, for GH occurring in a rather dispersed manner, could be accomplished by using P- and S-seismic wave attenuation as a tool for indirect geophysical quantification (Guerin and Goldberg, 2002; Priest et al. 2006; Best et al. 2013; Marin-Moreno et al., 2017).

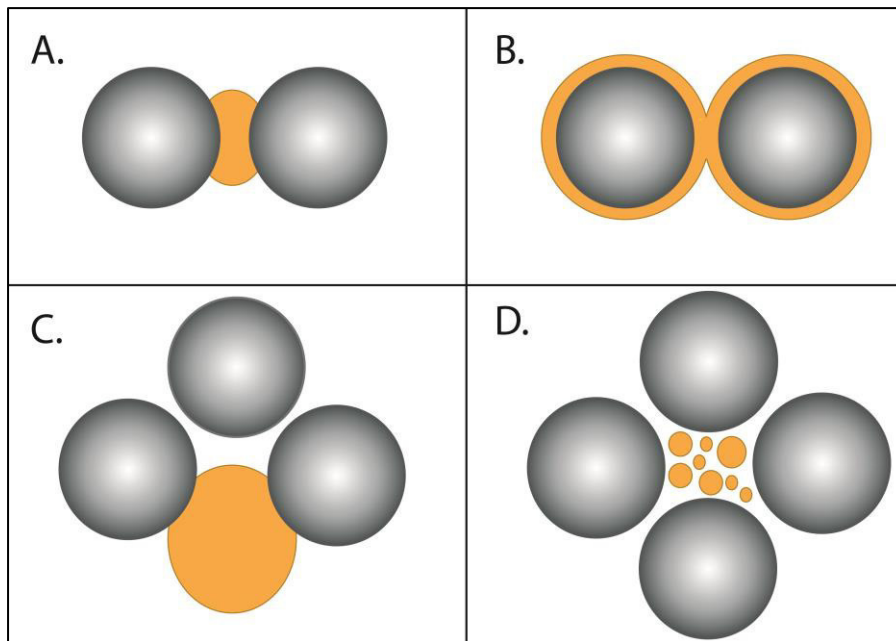
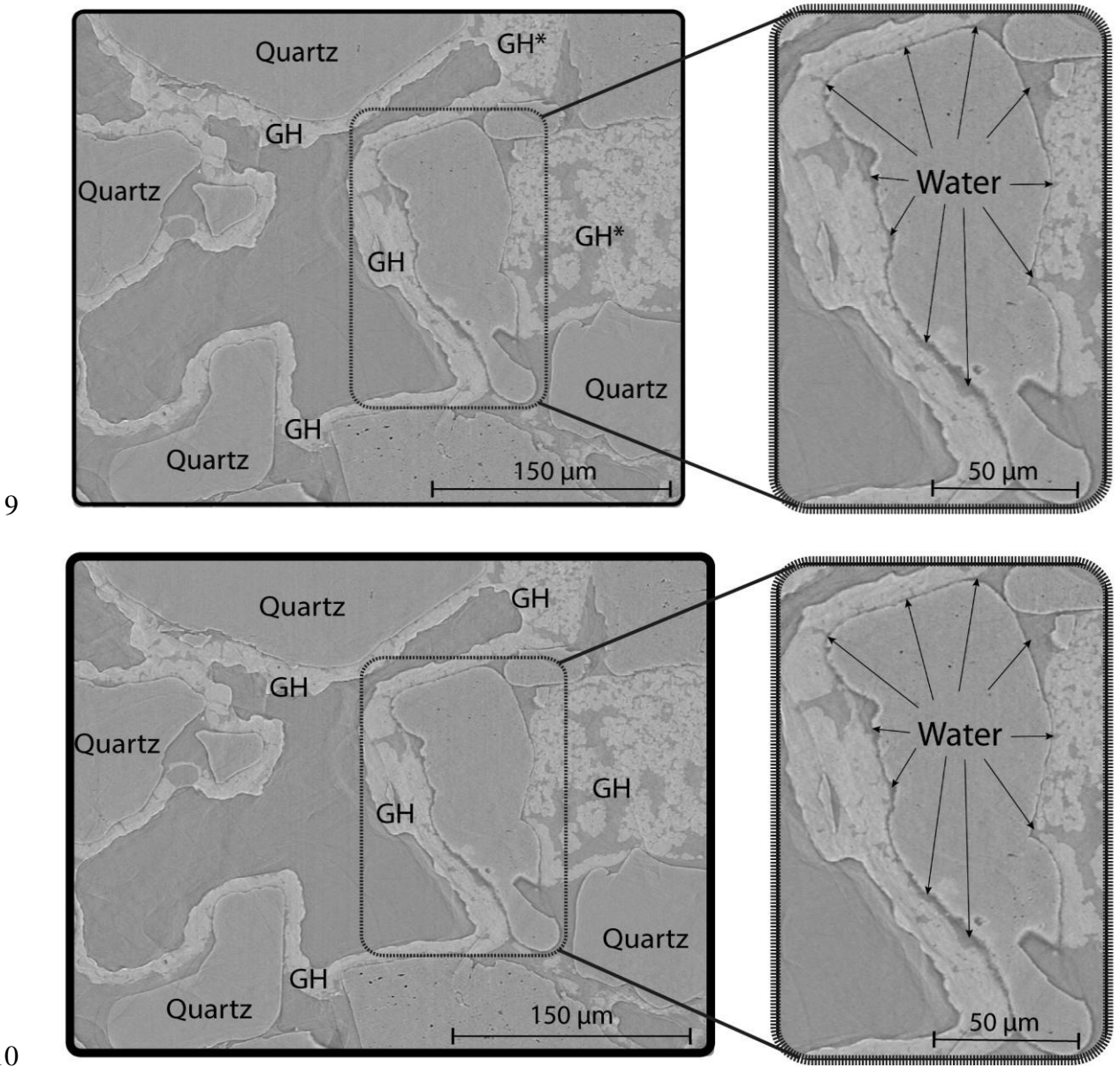


Figure 1. Review of the established conceptual models (Grains = grey and GH = orange), with (A) cementation – GH cements the grains, (B) encrustation – GH coats the grains, (C) matrix-supporting – GH is part of the sediment matrix, and (D) pore-filling – GH employs the pore space forming crystallites of varying size (modified after Dai et al., 2004).

1 **2. THE INTERFACIAL WATER FILMS**

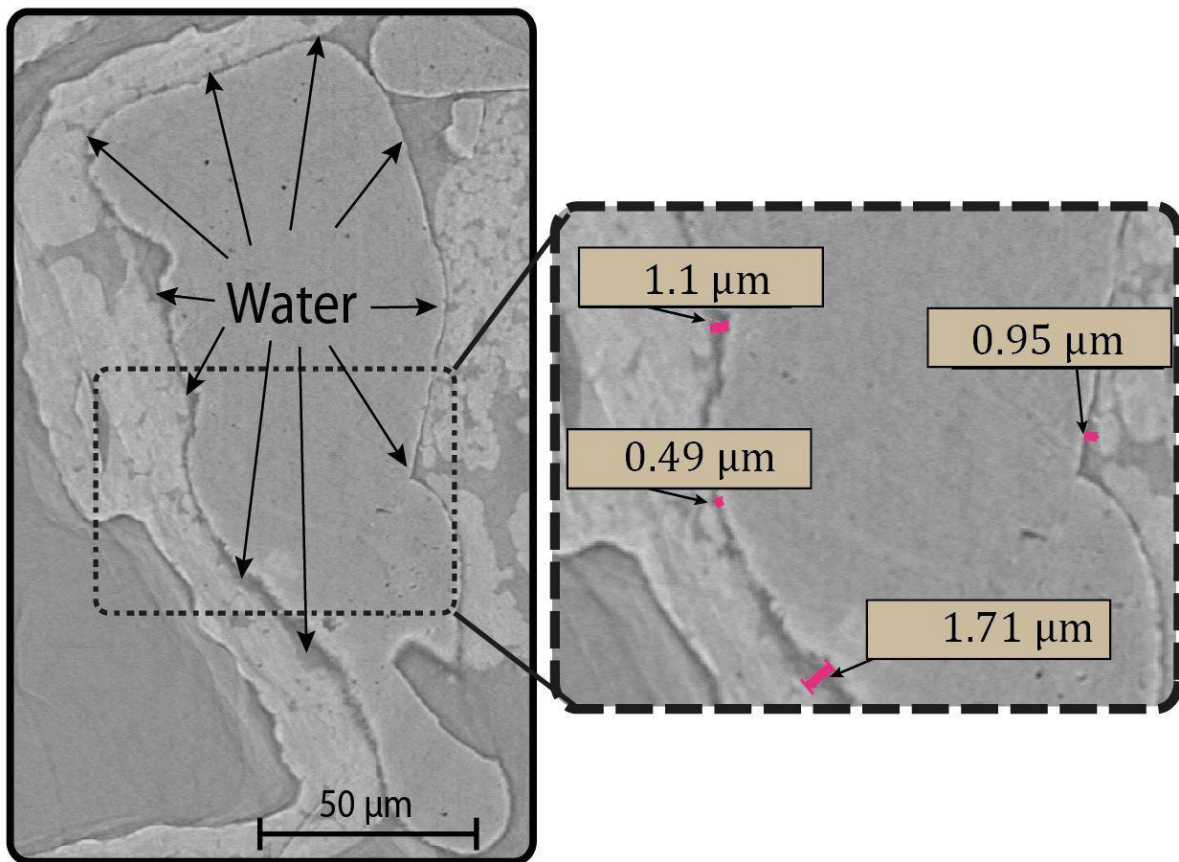
2 Chaouachi et al. (2015) conducted various in-situ experiments coupled with synchrotron-based
3 tomography at the TOMCAT beamline of the Paul Scherrer Institute in Villigen, Switzerland.
4 The aim was to study the formation process and distribution of gas hydrates in various matrices,
5 such as pure quartz sand and glass beads, as well as mixtures of quartz sand with clay minerals.
6 These in-situ experiments have been ~~realized~~ conducted using an experimental setup ~~under~~
7 elevated ~~that allowed for high~~ pressures and ~~lowered~~ temperatures. Further details are given by
8 Chaouachi et al. (2015), Falenty et al. (2015), and Sell et al. (2016).



11 **Figure 2.** (Left) Overview of an unfiltered 2D slice in y,z-direction of quartz sand containing GH. Note that due
12 to its unfiltered state, this image contains artifacts, such as streaks and slight edge enhancement. Phases can be
13 identified on the base of grey scale differences.

14 ~~In-For~~ this study, the 3D-micro-tomographySRXCT data obtained from the mentioned in--situ
15 experiments, are used ~~the focus lies~~ on samples containing pure natural quartz sand

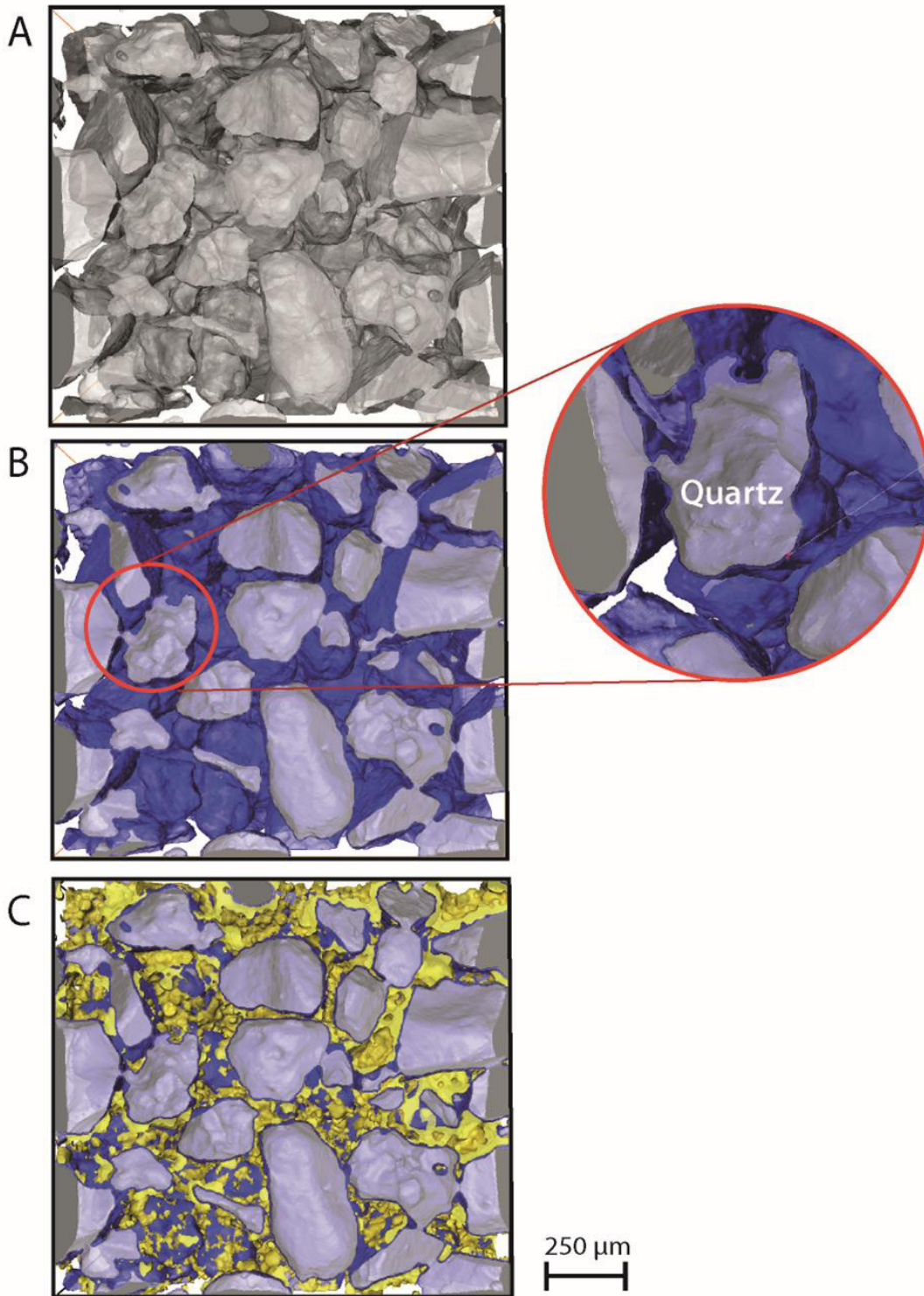
1 sieved at 200–300 μm grain size. ~~Details on the sedimentology and mineralogy of the host~~
2 ~~sediment are provided by~~ Chuvilin et al. (2011) ~~provides details on the sedimentology and~~
3 ~~mineralogy of the host sediment.~~ We use a reconstruction process (Marone and Stampanoni,
4 2012) that yields an image matrix of $2560 \times 2560 \times 2160$ voxels, with ~~an~~-isometric voxel sizes
5 of 0.74 and 0.38 μm at 10-fold and 20-fold optical magnification, respectively. The
6 reconstructed tomograms revealed discernible grey value differences between the three
7 relevant phases of the sample: solid grains, hydrate, and water (Figure 2). ~~The image analysis~~
8 ~~was has been accomplished~~ ~~T~~to reduce image artifacts, such as inhomogeneity in grey scale
9 values, streaks and edge enhancement, ~~we~~ by applying a systematic image enhancement
10 workflow comprising different image filter combinations in 2D and 3D (Sell et al., 2016). ~~One~~
11 ~~of the most interesting observations made was a~~ Chaouachi et al. (2015) observed ~~Aa~~ systematic
12 appearance of ~~an~~ thin interfacial water film separating the quartz grains from the GH phase
13 (~~Chaouachi et al., 2015~~). ~~This fluid interface was observed~~ in samples where GH was formed
14 ~~in quartz sand samples~~ directly from the juvenile state not involving GH dissociation, as well
15 as where GH was formed from ~~gas-enriched water~~ ~~the gas in excess method.~~ ~~This observation~~
16 ~~is in accordance with the publication of~~ Tohidi et al. (2001). ~~Additionally several molecular~~
17 ~~numerical simulations showed that a water layer prefers the interface of GH and quartz grains~~
18 (~~Bagherzadeh et al., 2012; Bai et al., 2011; Liang et al., 2011~~). ~~Identifying the water films and~~
19 ~~quantifying its thickness was one scope of this study to adapt our conceptual model.~~



20

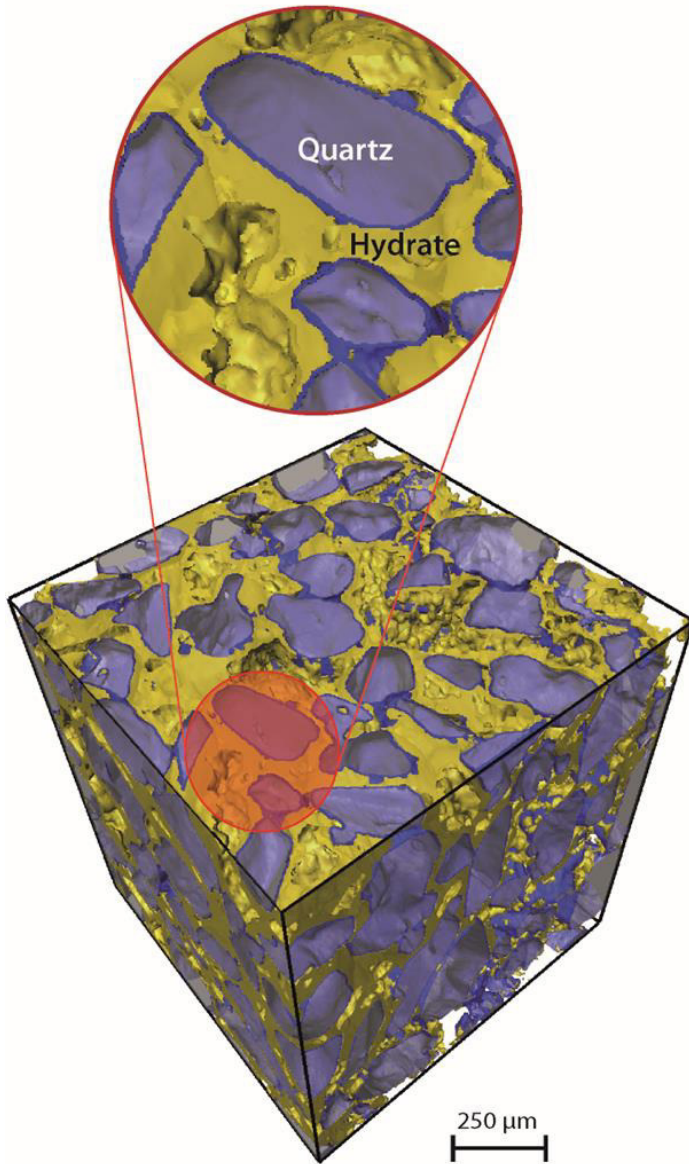
21 **Figure 3.** Raw (unfiltered) 2D image in y,z-direction at a spatial resolution of 0.38 μm . The zoom depicts
22 the measurement of a thin interfacial water film varying in thickness from 0.49 μm to 1.71 μm .

1 The broad range of grey scale values of the filtered images ~~can be~~ were classified using
2 watershed segmentation combined with region growing tools of the software packages of
3 Avizo Fire 7 (FEI, France) and Fiji. ~~The full workflow has been described by Sell et al. (2016).~~
4 ~~Basically, f~~For~~In the present study, is work we determined~~ the thickness variation and geometry
5 of the water film ~~has been determined~~ (Figure 3), ~~an information needed to define our~~
6 ~~conceptual model to investigate on attenuation in GH-bearing sedimentary matrices (Figure 6).~~
7 Following the image enhancement and segmentation process described by~~in~~ Sell et al. (2016),
8 the segmented data illustrate the characteristics and appearance of the phases distributed in the
9 samples (Figure 4). Moreover, the high resolution of the data enables us to obtain 3D images
10 in which particular details, like~~such as~~ water bridges connecting two interfacial water films,
11 are detectable (Figure 5). With information collected from the 3D data, our newly
12 introduced~~proposed~~ he multi-phase conceptual model ~~involves initially idealized round-~~
13 ~~shaped grains covered by a homogenous thin-water film which is in turn and can be adjusted~~
14 (i) to include grains embedded in non-porous hydrate. The conceptual model ~~or porous hydrate,~~
15 can be adjusted (ii) to include water bridges connecting the water films (Figure 6 and 12) and/or
16 (iii) isolated water pockets within the hydrate and separated from the water films.



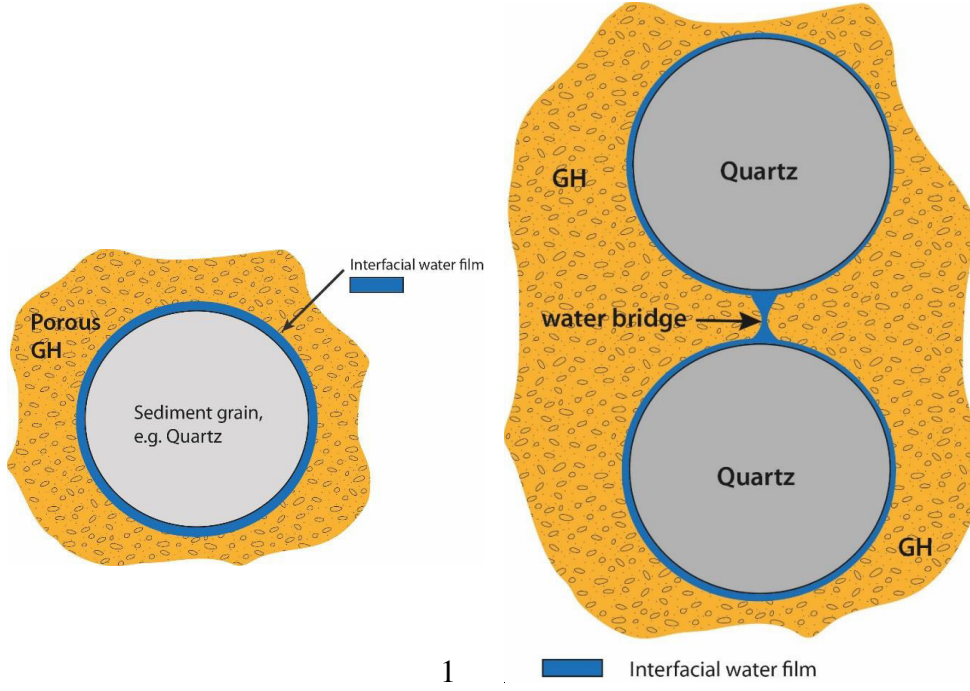
1

2 **Figure 4.** Volume-rendered phases in a representative image sample. For a better visualization, the
3 phases are introduced step-by-step, with (A) grains (grey), (B) grains and interfacial water films (blue),
4 and (C) grains, water film and hydrate (yellow). A zoom in (B) shows an interfacial water film measured
5 at 1 – 4 voxels equivalent to 0.38 – 1.52 μm thickness, respectively.



1

2 **Figure 5.** Volume-rendered image of a representative Region of interest (ROI) of $600 \times 600 \times 600$
3 voxels at $0.38 \mu\text{m}$ spatial resolution. The zoom-in depicts quartz grains fully separated from the pore-
4 filling hydrate by thin interfacial water films, with two quartz grains having their water films
5 interconnected by a water bridge.



2 **Figure 6.** Schemes of (A) a new concept model for GH encrusting quartz grains separated by a thin
 3 interfacial water film and (B) connected by a water bridge.

4

5 3. NUMERICAL METHODOLOGY

6 3.1 Mathematical formulation

7 To estimate frequency-dependent attenuation in the GH systems described above we employ a
 8 hydromechanical approach (Quintal et al., 2016) based on the conservation of momentum

$$9 \quad \nabla \cdot \boldsymbol{\sigma} = 0, \quad (1)$$

10 with the components σ_{kl} of the stress tensor $\boldsymbol{\sigma}$ defined according to the general stress-strain
 11 relations in the frequency domain

$$12 \quad \sigma_{kl} = 2\mu\varepsilon_{kl} + \left(K - \frac{2}{3}\mu \right) e\delta_{kl} + 2\eta\omega i\varepsilon_{kl} - \frac{2}{3}\eta\omega i e\delta_{kl}, \quad (2)$$

13 where ε_{kl} denotes the components of the strain tensor, e denotes the cubical dilatation given by
 14 the trace of the strain tensor, ω is the angular frequency, and i represents the unit imaginary
 15 number. The indexes $k, l = 1, 2, 3$ refer to the three Cartesian directions x_1, x_2, x_3 or x, y, z and
 16 δ_{kl} is the Kronecker delta ($\delta_{kl} = 1$ for $k = l$ and $\delta_{kl} = 0$ for $k \neq l$). The material parameters $\mu, K,$
 17 and η are the shear modulus, the bulk modulus, and the shear viscosity, respectively.

18 Using this general mathematical formulation (equations 1 and 2), a heterogeneous medium can
 19 be described as having an isotropic, linear elastic solid frame and fluid-filled cavities or pores,
 20 to which a specific choice of material parameters can be assigned. ~~The same unknowns and~~
 21 ~~material parameters describe the behaviors of the solid and the fluid phases. For example, an~~
 22 ~~unknown μ describes the solid displacement in the domains of the model representing an elastic~~

1 ~~solid and also describes the fluid displacement in the domains representing a viscous fluid. In~~
2 ~~fact, e~~Equation 2 reduces to Hooke's law by setting the shear viscosity η to zero in the solid
3 domains. In these regions, μ and K denote the shear and bulk moduli of the corresponding
4 elastic solid, ~~and the shear viscosity η is zero~~. In the fluid-filled model domains ~~representing a~~
5 ~~compressible viscous fluid~~, the shear modulus μ is set to zero while K and η denote the bulk
6 modulus and shear viscosity of the fluid. ~~In this domains~~ and the combined equations 1 and 2
7 reduce to the quasi-static, linearized Navier-Stokes' equations for the laminar flow of a
8 Newtonian fluid (e.g., Jaeger et al., 2007). ~~In these fluid-filled regions, K and η denote the bulk~~
9 ~~modulus and shear viscosity of the fluid~~.

10 When the aforementioned heterogeneous medium is deformed, fluid pressure differences
11 between neighbor regions induce fluid flow or, more accurately, fluid pressure diffusion, which
12 in turn results in energy loss caused by viscous dissipation (Quintal et al., 2016). At the
13 microscopic scale, this attenuation mechanism is commonly referred to as squirt flow (e.g.,
14 O'Connell and Budiansky, 1977; Murphy et al., 1986) and is the sole cause of attenuation in
15 our simulations, as we neglected the inertial terms in equations 1 and 2.

16 **3.2 Finite element modeling**

17 Our 2D problem is equivalent to a 3D case under plain strain conditions, which means no strain
18 outside the modeling plane is allowed to develop. For the corresponding simulations, we
19 consider the directions x and y , to be in the modeling plane and direction z to be the one in
20 which no displacement or displacement gradients can occur.

21 The numerical solution is based on a finite-element approach in the frequency domain. We
22 employ an unstructured triangular mesh, which allows for an efficient discretization of slender
23 heterogeneities having large aspect ratios, such as the thin interfacial water films, by strongly
24 varying the sizes of the triangular elements (e.g., Quintal et al., 2014). A few elements across
25 the thin interfacial water film are necessary to accurately capture the viscous dissipation in this
26 region, while much larger elements are sufficient in the solid elastic domains. The sizes of
27 smallest and largest elements in our meshes differ by 3 orders of magnitude.

28 To assess the P-wave attenuation and modulus dispersion caused by squirt-flow, we subject a
29 rectangular numerical model to an oscillatory test. A sinusoidal downward displacement is
30 applied homogeneously at the top boundary of the numerical model. At the bottom, the
31 displacement in the (y) vertical direction is set to zero. At the lateral boundaries of the model,
32 the displacement in the (x) horizontal direction is set to zero. From this test, we obtain the stress
33 and strain fields, averaged over the entire model domain. The mean stress and strain are used
34 to compute the complex-valued and frequency-dependent P-wave modulus corresponding to a
35 wave propagating in the vertical direction. The real part of the P-wave modulus H is used to
36 illustrate the P-wave modulus dispersion while the ratio between its imaginary and real parts
37 is used to quantify the P-wave attenuation $1/Q_P$. The S-wave attenuation and dispersion can be
38 evaluated in a similar manner ~~simply~~ by changing the boundary conditions to those of a simple-
39 shear test (e.g., Quintal et al., 2012, 2014).

40

1 ~~Our 3D problem is solved s~~Similarly to the 2D problem, the solution to our 3D problem
2 using a basis based on the application of an unstructured mesh, ~~but~~ with tetrahedral elements.
3 ~~Again, t~~The element sizes in our 3D meshes also vary by about 3 orders of magnitude.

4. NUMERICAL RESULTS

7 Many sources of squirt flow might coexist in unconsolidated sediments hosting GH, such as
8 those resembling the conventional squirt flow models introduced by O'Connell and Budiansky
9 (1977) for interconnected microcracks and by Murphy et al. (1986) for microcracks or grain
10 contacts connected to spherical pores. Marin-Moreno et al. (2017) describes an integrated
11 approach that combines the effects of some squirt flow models and other attenuation
12 mechanisms. Here our objective diverges from that. We instead aim at studying the squirt flow
13 phenomenon and the resulting frequency-dependent attenuation associated with a specific
14 model, which is geometrically different from the mentioned conventional squirt flow models
15 and is based on the thin interfacial water films. We thus neglect all other potentials sources of
16 attenuation.

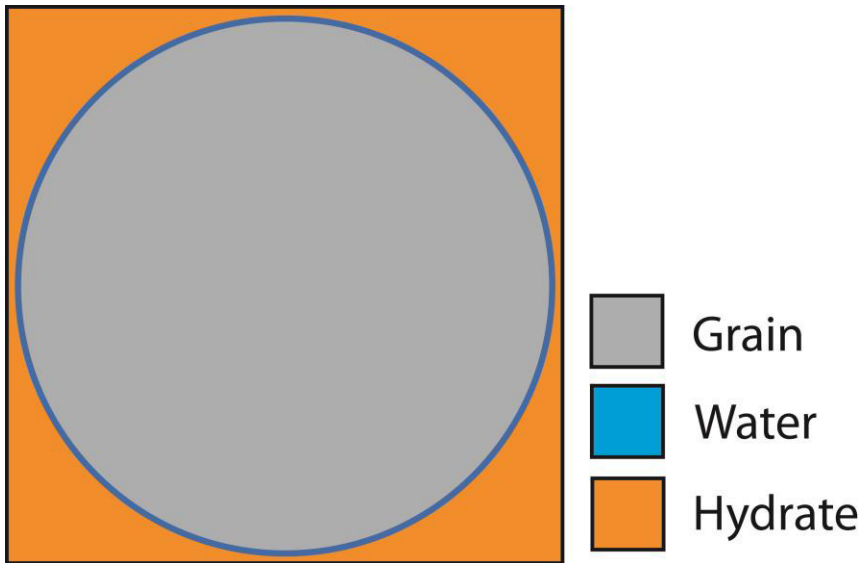
4.1 Attenuation mechanism in a thin interfacial water film

19 Our 2D numerical model domain corresponds to a fundamental block of a periodic distribution
20 of unconsolidated circular quartz grains dispersed in a continuous GH background and
21 separated from the latter by a thin interfacial water film (Figure 7). ~~Aim of this basic model is~~
22 ~~to have a first estimate of the possible attenuation effect by a thin interfacial water film.~~ The
23 subdomain representing the thin interfacial water film is described by the corresponding
24 properties of this viscous fluid, while the other subdomains are described by properties of two
25 different elastic solids, quartz and GH. These properties are given in Table 1 and the numerical
26 mesh is shown in Figure 8.

27 ~~Based on the material properties given in Table 1, w~~We consider thicknesses of the interfacial
28 water film ranging from 0.1 μm to 1 μm as well as two grain diameters 150 and 250 μm for the
29 2D model. These values were chosen considering the sizes of the quartz grains used in the
30 laboratory experiment from which the SRXCT data were obtained, which ranged from 150 to
31 300 μm , and the thicknesses of the interfacial water films observed in the data, ranging from
32 0.38 μm to 1.5 μm . Note that the thinnest interfacial water films observed were limited by the
33 highest achieved spatial resolution of 0.38 μm . Despite ~~this limitation of spatial resolution, the~~
34 water film thicknesses below 0.38 μm have also been considered for our numerical analysis ~~as~~
35 ~~well.~~

36 The numerical results are expressed as the real part of the P-wave modulus and the P-wave
37 attenuation $1/Q_P$ (Figure 9-8). We observe that a decrease in the thickness of the interfacial
38 water film causes the attenuation and dispersion curves to shift to lower frequencies. In fact,
39 high attenuation values ($1/Q \sim 0.1$) are observed at seismic frequencies (~ 100 Hz) when the

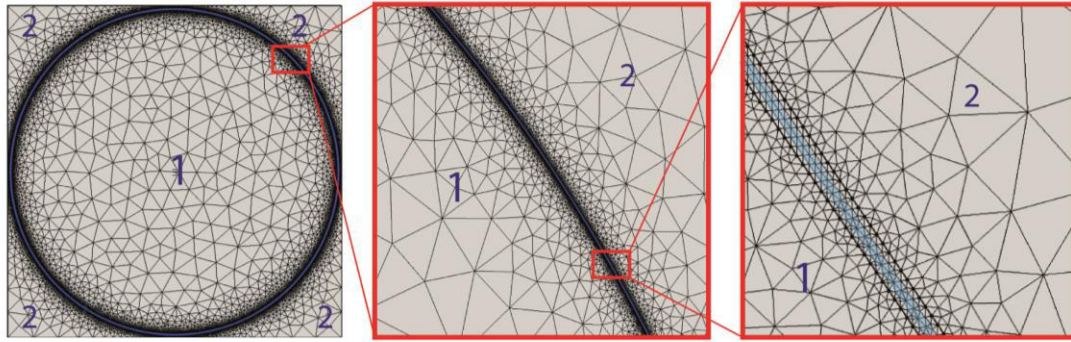
1 interfacial water film is as thin as 0.1 μm and the grain diameter is as large as 250 μm .
 2 Decreasing the grain diameter, ~~on the other hand,~~ causes a shift to higher frequencies of the
 3 attenuation and dispersion curves.



4
 5 **Figure 7.** Fundamental block of an idealized periodic medium representing -sediment grains which are
 6 separated from the embedding GH background by a thin interfacial water film.

7
 8 **Table 1.** Material properties used in the numerical simulations. *The properties of quartz are based on
 9 the work of Bass (1995) and those of hydrate on Helgerud (2003).

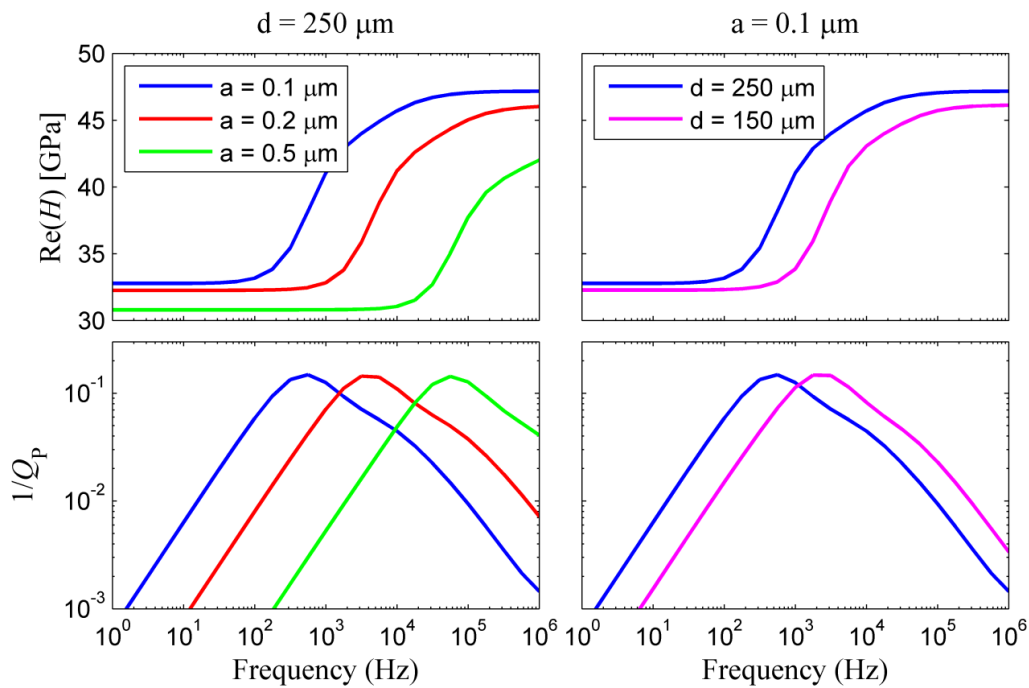
Material parameter	Quartz*	Hydrate*	Water
Shear modulus μ	44.3 GPa	13.57 GPa	0
Bulk modulus K	37.8 GPa	8.76 GPa	2.4 GPa
Shear viscosity η	0	0	0.003 Pa·s



1

2 **Figure 8.** The triangular mesh used for the numerical model shown in Figure 7. To distinguish between
 3 the phases: Quartz is denoted with # 1, GH is denoted with # 2 and the interfacial water film is depicted
 4 in a light-blue color.

5



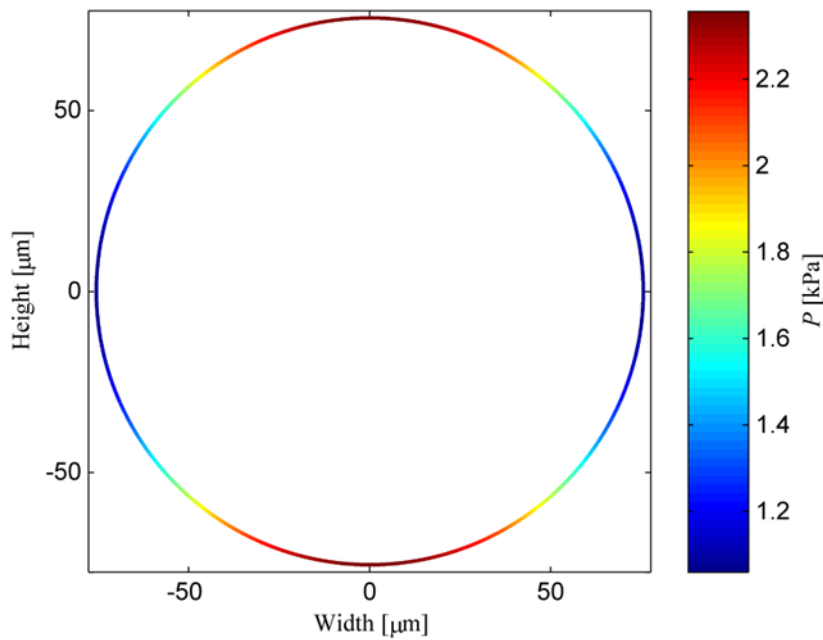
6

7 **Figure 9-8.** Real part of P-wave modulus, H , and corresponding P-wave attenuation, $1/Q_P$, as functions
 8 of frequency, for the model shown in Figure 7, considering the grain diameter d and thickness a of the
 9 interfacial water film, which are indicated in the legends and plot titles.

10 The geometry of the introduced model (Figure 7) is different than the classical squirt-flow
 11 geometries involving interconnected plane cracks or a plane crack connected to a pore of low
 12 aspect ratio. To better understand how dissipation occurs for this type of geometry, we initially
 13 focus on the fluid pressure field P (Figure 109) in the circular interfacial water film at the
 14 characteristic frequency. The vertical compression of the model illustrated in Figure 7 causes
 15 a larger deformation of the interfacial water film at the top and bottom ~~of its circular~~
 16 ~~geometry parts~~ than on the ~~lateral parts~~ sides. This observation is comparable to horizontal
 17 cracks that are more deformed by a vertical compression than vertical cracks in a classical
 18 squirt flow model. Here, the heterogeneous deformation causes fluid pressure to increase. The

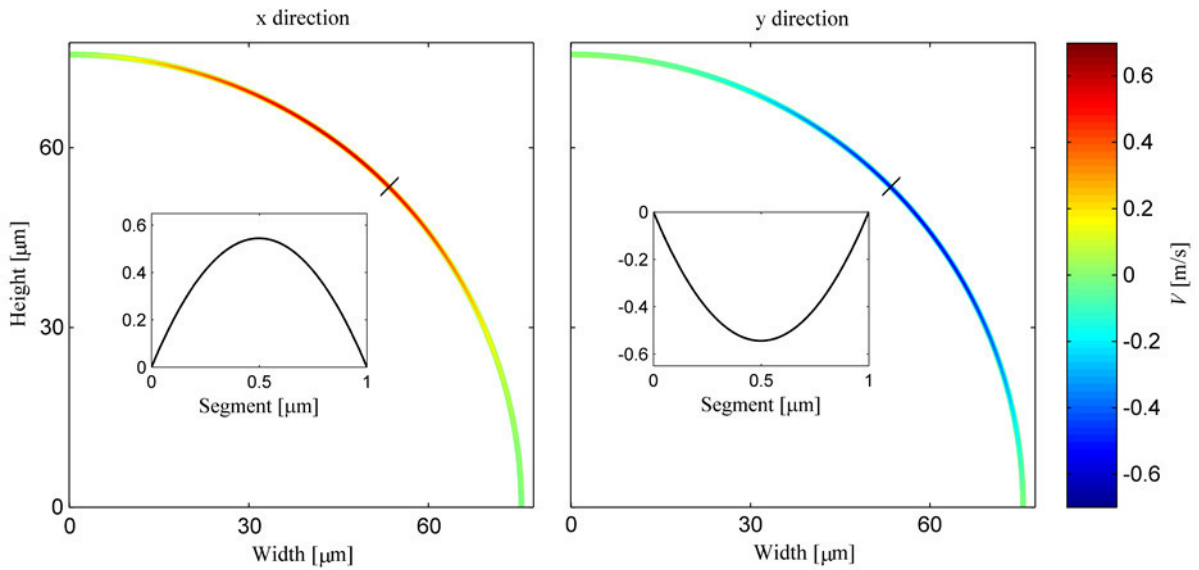
1 most deformed parts which are the top and the bottom, exhibit the highest fluid pressure, as
 2 shown in Figure 109. The pressure gradient present in this heterogeneous pressure field induces
 3 fluid to be displaced from the regions of higher pressure (top and bottom) towards the regions
 4 of lower pressure (left and rightsides). Exemplarily, the components of the fluid velocity field
 5 in the x and y directions V_x and V_y (Figure 110) and its the corresponding local attenuation field
 6 $1/q$ (Figure 112) are depicted in only the representative top-right quadrant of the model.
 7 Considering the symmetry of this process in the four quadrants of the circular interfacial water
 8 film (Figure 109) it is reasonable sufficient to show only one quadrant out of four.

9 In Figure 110 we observe the text-book (e.g., Jaeger et al., 2007) parabolic profile of the fluid
 10 velocity across the interfacial water film, with larger fluid velocity in the center of the film,
 11 governed by Navier-Stokes equations. This fluid velocity is associated with an energy
 12 dissipation caused by viscous friction, shown in Figure 112. At the boundaries of the interfacial
 13 water film, larger viscous friction explains the lower fluid velocity and larger energy
 14 dissipation, in comparison to the center of the film. The attenuation is strongly reduced towards
 15 the center of the film by a few orders of magnitude. Now looking at how these fields change
 16 along the interfacial water film, we observe that the maximal velocity and attenuation (compare
 17 Figures 110 and 112) coincide with the maximal pressure gradient (Figure 109). Whereas on
 18 the other hand, in the middle of the higher pressure and lower pressure regions, the pressure
 19 gradient is minimal causing the fluid velocity and attenuation to drop drastically.



20

21 **Figure- 109.** Fluid pressure P for the model shown in Figure 7, considering a grain diameter $d = 150$
 22 μm and thickness of the interfacial water film $a = 1 \mu\text{m}$. The oscillation frequency is equal to the
 23 characteristic frequency ($1.8 \times 10^6 \text{ Hz}$).



1

2

3

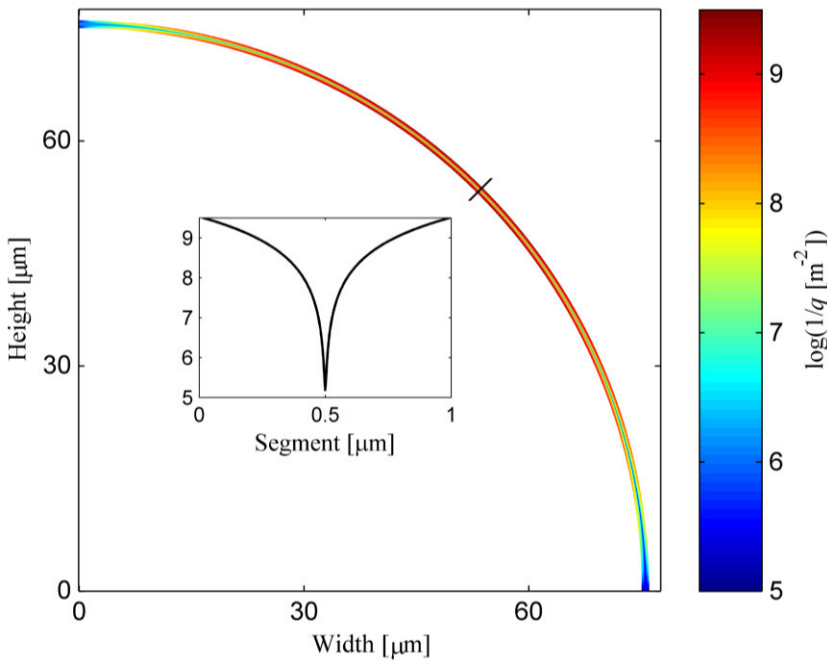
4

5

6

7

Figure 10 11. Zoom-in to the top-right quadrant of the model shown in Figure 9 showing the fluid velocity components V_x and V_z , for a grain diameter $d = 150 \mu\text{m}$, a thickness of the interfacial water film $a = 1 \mu\text{m}$, and at the characteristic frequency. These fields correspond to the fluid pressure field shown in Figure 109. The insets illustrate the profiles across the interfacial film where it is crossed by a black line.



8

9

10

11

12

13

14

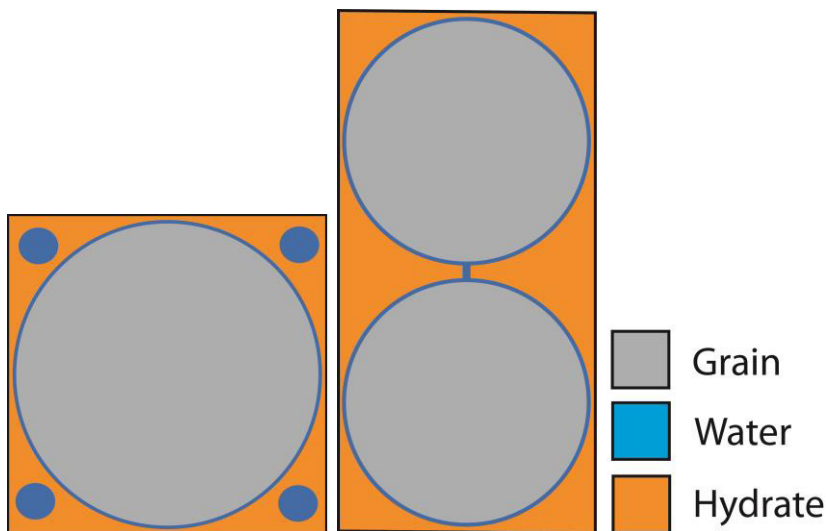
Figure 11 12. Zoom-in to the top-right quadrant of the model shown in Figure 7 showing the local attenuation $1/q$, for a grain diameter $d = 150 \mu\text{m}$, with a water film thickness $a = 1 \mu\text{m}$, and at the characteristic frequency. This field corresponds to those shown in Figures 109 and 101. The inset illustrates the profile across the interfacial film where it is crossed by a black line.

1 4.2 Effects of water pockets and water bridges

2 In this subsection, a few alterations are added to the basic ~~three-phase~~ model illustrated in
3 Figure 7. These alterations ~~are based~~ on more detailed observations obtained from SRXCT,
4 such as water pockets ~~that have been detected~~ in non-porous GH or a water bridge that might
5 occur connecting two neighboring interfacial water films (Figure 123). For this, the effect of
6 these features on the P-wave modulus dispersion and attenuation (Figure 134) is studied and
7 compared to results obtained from corresponding models where these features have not been
8 considered.

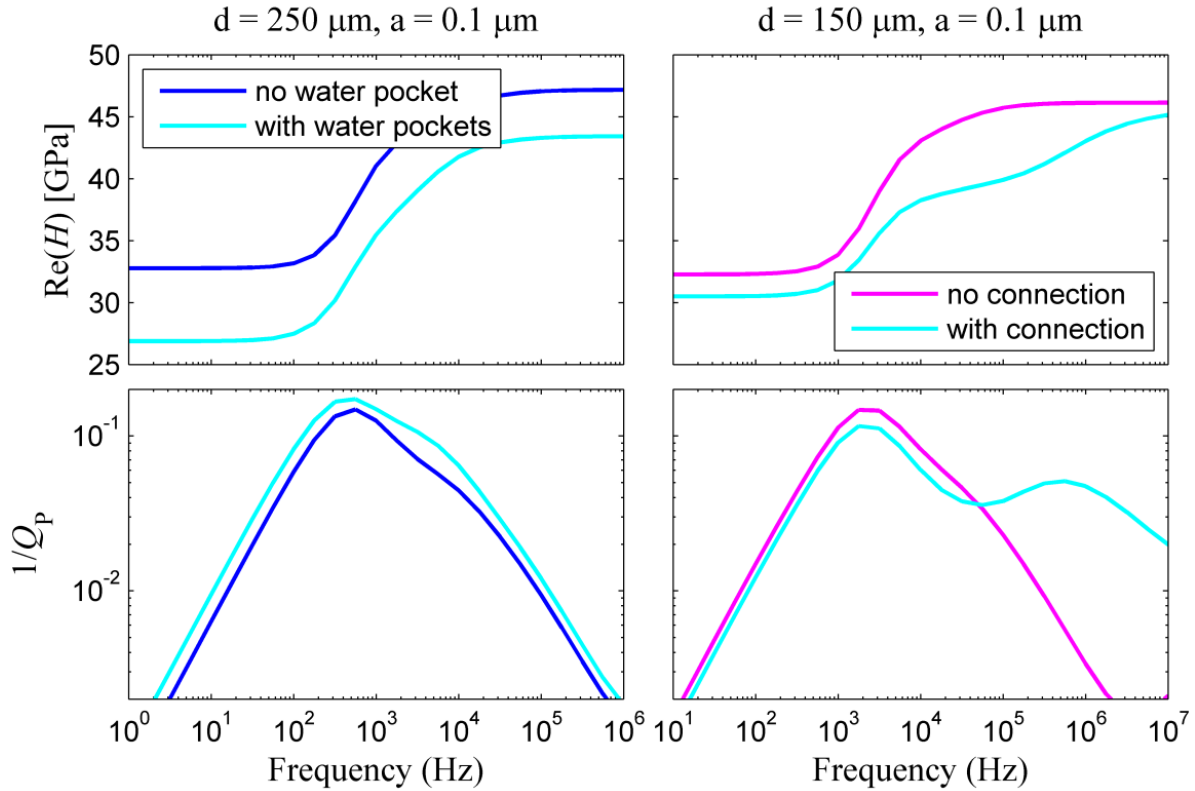
9 The inclusion of water pockets has a modest effect on the attenuation and dispersion, while it
10 reduces the overall value of the P-wave modulus, as a certain volume of GH is replaced by a
11 much less stiff material (water). Concurrently,The modest increase in attenuation is associated
12 with a more compressible effective background; no attenuation occurs within the water
13 pockets.

14 The connecting water bridge introduces an additional length scale for the dissipation process,
15 as fluid flow and dissipation will also occur through this relatively short and wide path. This
16 explains the additional attenuation peak observed at higher frequencies, while the previous
17 peak at 2×10^3 Hz suffers a slight reduction in magnitude. A reduction in magnitude occurs
18 because the pressure equilibration process involving the water bridge causes a reduction in
19 pressure in the region connected to the bridge and thus a reduction of the previously discussed
20 (Figure 98) pressure gradient between this region and the sides of the circular interfacial water
21 film. The dispersion agrees with the attenuation curve, with two inflections, corresponding to
22 the two attenuation peaks; between the high- and low-frequency limits.



24 **Figure 132.** Fundamental blocks of two periodic media representing loose sandstone grains which are
25 separated from the embedding GH background by a thin interfacial water film. On the left water pockets
26 are located in the GH background and on the right the interfacial water films are connected to another
27 through a water bridge.

28



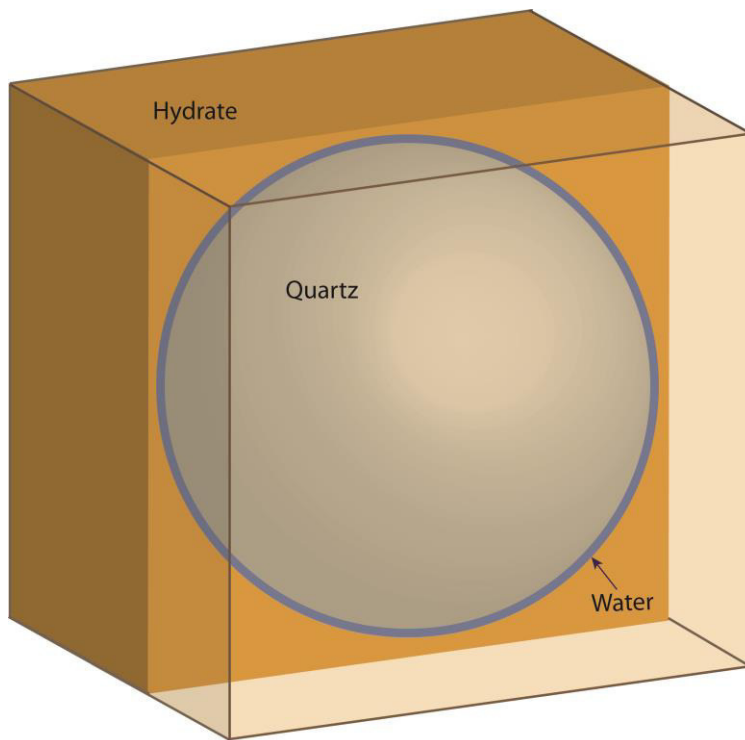
1

2 **Figure 143.** Real part of P-wave modulus, H , and corresponding P-wave attenuation, $1/Q_p$, as functions
 3 of frequency, for the models shown in Figure 123 in comparison with the corresponding results from
 4 the model shown in Figure 7 and given in Figure 98. The grain diameter d and thickness a of the
 5 interfacial water film are indicated in the plot titles.

6

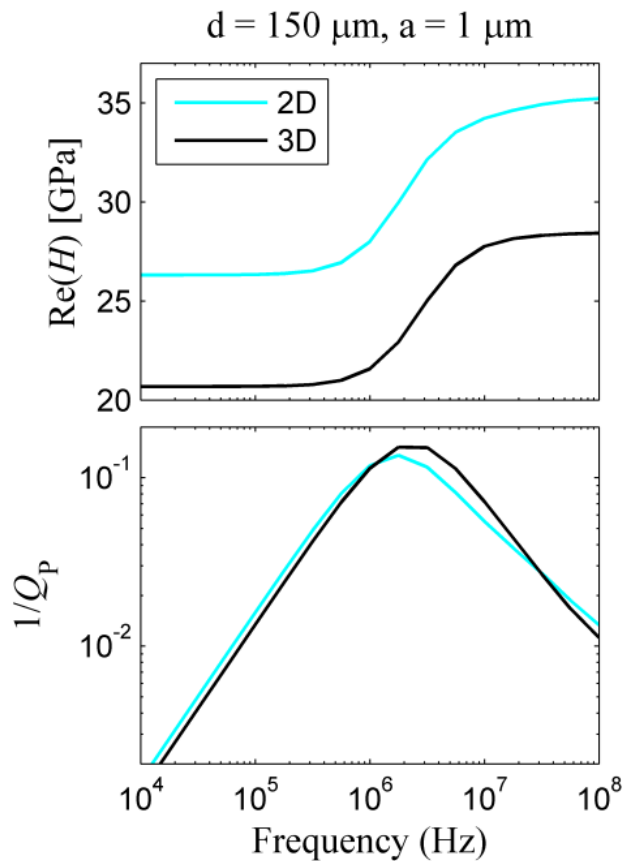
7 4.3 Evaluation of 3D effects

8 The following subsection considers a comparison between the results of the simulation
 9 illustrated in Figures 109-124, for the 2D model shown in Figure 7, and those of a simulation
 10 performed on its 3D counterpart. Our 3D model consists of a sphere in the middle of a cube
 11 (Figure 154), ~~consequently for which~~ a centered cross section matches the 2D model shown in
 12 Figure 7. The ~~aperture thickness~~ of the water film is $1\ \mu\text{m}$ and the grain diameter is $150\ \mu\text{m}$ (as
 13 for Figures 910-124). The numerical results are shown in Figure 156 with an excellent
 14 agreement between the results from the 2D and 3D models in terms of magnitude and
 15 characteristic frequency of attenuation. Indeed this was expected due to the radial symmetry of
 16 the spherical interfacial water film. This outcome indicates that 3D effects are small for the
 17 adopted geometry. ~~Furthermore,~~ The results based on simple 2D models approximate well
 18 ~~according to~~ the dissipation magnitude and frequency dependence of their corresponding 3D
 19 scenarios. The difference in the overall value of the real-valued ~~Young's P-wave~~ modulus is
 20 associated with a larger relative quantity of soft GH and a lower relative quantity of stiff quartz
 21 in the 3D model.



1

2 **Figure 154:** The 3D counterpart of the model shown in Figure 7: Fundamental block of a periodic
3 medium representing unconsolidated quartz grains which are separated from the embedding GH
4 background by a thin interfacial water film.
5



1

2 **Figure 156.** Real part of P-wave modulus, H , and corresponding P-wave attenuation, $1/Q_P$, as functions
 3 of frequency, for the 2D model shown in Figure 7 and for its 3D counterpart shown in Figure 154. The
 4 grain diameter d and thickness a of the interfacial water film are indicated in the plot title. The fields
 5 shown in Figures 109-124 correspond to this 2D simulation.

6

7 **5. CONCLUSIONS**

8 ~~Thin~~ Interfacial water films between sediment grains and the embedding GH matrix ~~have were~~
 9 recently ~~been~~—observed in GH-bearing sediments through synchrotron-based micro-
 10 tomography at a spatial resolution down to $0.38 \mu\text{m}$. Based on these data, ~~we have determined~~
 11 the appearance and thicknesses of ~~such thin interfacial water films have been (geometrically)~~
 12 ~~determined~~. With this knowledge, a new conceptual squirt flow model, which refers to a
 13 spherical ~~thin fluid water~~ film coating the solid grains, was introduced ~~for GH-bearing~~
 14 ~~sediments~~. This geometry differs ~~e novelty of this model is constituted with respect to its~~
 15 ~~geometry, as compared to from the~~ classical squirt flow models ~~that involving interconnected~~
 16 microcracks, ~~interconnected~~ or ~~microcracks~~ connected to spherical pores ~~instead of interfacial~~
 17 ~~fluid films~~. Numerical simulations were performed to calculate the energy dissipation in the
 18 proposed model, considering a range of scenarios. Our results show that squirt flow in ~~thin~~
 19 ~~spherical~~ interfacial water films can cause large and frequency-dependent P-wave attenuation
 20 in a broad frequency range including seismic frequencies. ~~Additionally, this effect does depend~~
 21 ~~upon the interfacial water films being connected to any other type of pore.~~

1 ~~The~~A numerical ~~solution scheme is~~ based on a set of coupled equations that reduce to Hooke's
2 law in the subdomains of the model corresponding to the elastic solid materials (grains and
3 GH) and to the quasi-static, linearized Navier-Stokes equations in the subdomains
4 corresponding to the fluid (water)-~~has been used~~. The results for our conceptual model show
5 that the P-wave attenuation peak is shifted to lower frequencies with decreasing thickness of
6 the interfacial water film and with increasing grain size (or the length of the film), as
7 analogously known for the microcrack aperture and length in classical squirt flow models.
8 Furthermore, we tested the effect of inserting water pockets in an embedding GH matrix and
9 the effect of connecting two neighboring ~~thin~~-interfacial water films through a water bridge. In
10 general, the water bridges have a stronger effect on energy dissipation than the water pockets.
11 Introducing such connections between neighboring interfacial water films causes a broadening
12 of the P-wave attenuation spectrum towards higher frequencies. On the other hand, the presence
13 of water pockets in the GH background only causes a slight overall increase in P-wave
14 attenuation. Although the majority of our simulations were performed for 2D models,
15 ~~additional~~ results of a 3D simulation showed that 3D effects are small for the basic 2D models
16 that we have considered.

17 Our results represent a strong base to explain fundamental processes in GH-bearing sediments
18 and support previous speculations (Guerin and Goldberg, 2002; Dvorkin and Uden, 2004,
19 Priest et al., 2006) that squirt flow is an important attenuation mechanism in GH-bearing
20 sediments such media, even at frequencies as low as those in the seismic range. This strengthens
21 the perception that P-wave attenuation may be used as an indirect geophysical attribute to
22 estimate GH saturation. Nevertheless, further studies considering more realistic geometries for
23 the microstructure of GH bearing sediments are necessary for a successful strategy to estimate
24 GH saturations where hydrate is distributed in a dispersed manner instead of massive layers.
25 ~~This study simply represents the first attempt to understand P-wave attenuation in~~
26 ~~unconsolidated sediments having large simple structures investigating on grains embedded in~~
27 ~~GH and occurs in reservoirs of GH saturations around 90%.~~ For ~~such~~ a following study, our
28 aim is to implement the segmented 3D images obtained from synchrotron-based micro-
29 tomography as a direct model input for numerical investigations ~~whereby realistic ,considering~~
30 ~~also grain-to-grain contacts will be taken into account. Depending on the number and sizes of~~
31 ~~the grain-to-grain contacts Q, as a ratio of the imaginary part and the real part of the complex~~
32 ~~modulus, will change. T~~~~At the moment this approach~~~~he step towards more realistic structures~~
33 ~~as a model input~~ is challenging due to the corresponding large computational demand.
34 ~~Furthermore, such model input d and it and~~ requires additional segmentation steps for the 3D
35 images ~~that, such as to~~ allow for a smoothing of the stairs-like resolution artifacts at the
36 boundaries of the interfacial water films. ~~Furthermore, the image segmentation bears~~
37 ~~significant errors concerning the accuracy of the film thickness. With these future steps, our~~
38 ~~model will involve effects of a varying grain skeleton and different GH appearances as~~
39 ~~observed in laboratory samples and in nature.~~

41 ACKNOWLEDGEMENTS

1 The authors thank the staff of the GZG crystallography group headed by Prof. W.F. Kuhs of
2 the Georg August University Göttingen for their collaboration during the in-situ experiments
3 at the TOMCAT beamline (Paul Scherrer Institute in Villigen, Switzerland) in 2012 and 2013.
4 The presented work was co-funded by the German Science Foundation (DFG grant Ke 508/20
5 and Ku 920/18).

6

7 REFERENCES

8 Adelinet, M., J. Fortin, Y. Guéguen, A. Schubnel, and L. Geoffroy, (2010), Frequency and
9 fluid effects on elastic properties of basalt: Experimental investigations: Geophysical Research
10 Letters, 37, L02303, doi: 10.1029/2009GL041660.

11 [Bagherzadeh, S. A., P. Englezos, S. Alavi, and J. A. Ripmeester \(2012\) Molecular modeling](#)
12 [of the dissociation of methane hydrate in contact with a silica surface. J. Phys. Chem. B, 116,](#)
13 [3188–3197, Doi: 10.1021/jp2086544.](#)

14
15 [Bai, D., G. Chen, X. Zhang, and W. Wang \(2011\) Microsecond molecular dynamics](#)
16 [simulations of the kinetic pathways of gas hydrate formation from solid surfaces. Langmuir,](#)
17 [27, 5961–5967, Doi:10.1021/la105088b.](#)

18
19 Bass, J. D. (1995), Elasticity of Minerals, Glasses and Melts, In: Mineral physics and
20 crystallography: a handbook of physical constants, edited by T. J. Ahrens, pp. 45-63, American
21 Geophysical Union, Washington D.C., USA.

22
23 Berge, L. I., K. A. Jacobsen, and A. Solstad (1999), Measured acoustic wave velocities of R11
24 (CCl3F) hydrate samples with and without sand as a function of hydrate concentration, J.
25 Geophys. Res.-Solid Earth, 104(B7), 15415-15424.

26
27 Bellefleur, G., M. Riedel, T. Brent, F. Wright, and S. R. Dallimore (2007), Implication of
28 seismic attenuation for gas hydrate resource characterization, Mallik, Mackenzie Delta,
29 Canada, J. Geophys. Res., 112, B10311, doi:10.1029/2007JB004976.

30
31 Best, A., J. Priest, and C. Clayton (2010), A Resonant Column Study of the Seismic Properties
32 of Methane-Hydrate-Bearing Sand, in Geophysical Characterization of Gas Hydrates, edited
33 by M. Riedel, E. C. Willoughby and S. Chopra, pp. 337-347, Society of Exploration
34 Geophysicists.

35
36 Best, A. I., J. A. Priest, C. R. I. Clayton, and E. V. L. Rees (2013), The effect of methane
37 hydrate morphology and water saturation on seismic wave attenuation in sand under shallow
38 sub-seafloor conditions, Earth Planet. Sci. Lett., 368, 78-87.

39
40 Biot, M. A., 1962, Mechanics of deformation and acoustic propagation in porous media:
41 Journal of Applied Physics, 33, 1482-1498, doi: 10.1063/1.1728759.

42 Bohrmann, G. T. M. E. (2006), Gas Hydrates in Marine Sediments, in Marine Geochemistry,
43 edited, pp. 481-512, Springer Berlin Heidelberg.

44

1 Brajanovski, M., B. Gurevich, and M. Schoenberg, 2005, A model for P-wave attenuation and
2 dispersion in a porous medium permeated by aligned fractures, *Geophysical Journal*
3 *International*, 163, 372–384, doi: 10.1111/j.1365-246X.2005.02722.x.

4 Chaouachi, M., A. Falenty, K. Sell, F. Enzmann, M. Kersten, D. Haberthür, and W. F. Kuhs
5 (2015), Microstructural evolution of gas hydrates in sedimentary matrices observed with
6 synchrotron X-ray computed tomographic microscopy, *Geochemistry, Geophysics,*
7 *Geosystems*, 16(6), 1711–1722.

8

9 Chapman S., Tisato N., Quintal B., Holliger K. (2016), Seismic attenuation in partially
10 saturated Berea sandstone submitted to a range of confining pressures. *Journal of Geophysical*
11 *Research - Solid Earth*, 121(3):1664–1676, doi: 10.1002/2015JB012575.

12

13 Chuvilin, E. M., V. A. Istomin, and S. S. Safonov (2011), Residual nonclathrated water in
14 sediments in equilibrium with gas hydrate Comparison with unfrozen water, *Cold Reg Sci*
15 *Technol*, 68(1-2), 68-73.

16

17 Collett, T. S. a. L., John (2000), 19. Detection of gas hydrate with downhole logs and
18 assessment of gas hydrate concentrations (saturations) and gas volumes on the Blake Ridge
19 with electrically resistivity log data. *Proceedings of the Ocean Drilling Program. Scientific*
20 *Results*, 164.

21

22 Dai, J., H. Xu, F. Snyder, and N. Dutta (2004), Detection and estimation of gas hydrates using
23 rock physics and seismic inversion: Examples from the northern deepwater Gulf of Mexico,
24 *The Leading Edge*, 23(1), 60-66.

25

26 Dai, S., J. C. Santamarina, W. F. Waite, and T. J. Kneafsey (2012), Hydrate morphology:
27 Physical properties of sands with patchy hydrate saturation, *J. Geophys. Res.-Solid Earth*, 117,
28 12.

29

30 Dewangan, P., R. Mandal, P. Jaiswal, T. Ramprasad, and G. Sriram (2014), Estimation of
31 seismic attenuation of gas hydrate bearing sediments from multi-channel seismic data: A case
32 study from Krishna-Godavari offshore basin, *Mar. Petrol. Geol.*, 58, 356–367.

33

34 Dvorkin, J., A. Nur, R. Uden, and T. Taner (2003), Rock physics of a gas hydrate reservoir,
35 *The Leading Edge*, 22(9), 842-847.

36

37 Dvorkin, J. and Uden, R. (2004), Seismic wave attenuation in a methane hydrate reservoir, *The*
38 *Leading Edge*, 23(8), 730-732.

39

40 Ecker, C., J. Dvorkin, and A.M. Nur (1998), Sediments with gas hydrates: Internal structure
41 from seismic AVO, *Geophysics* 63(5), 1659-1669.

42

43 Ecker, C., J. Dvorkin, and A. M. Nur (2000), Estimating the amount of gas hydrate and free
44 gas from marine seismic data, *Geophysics*, 65(2), 565-573.

45

46 Falenty, A., M. Chaouachi, S. H. Neher, K. Sell, J.-O. Schwarz, M. Wolf, F. Enzmann, M.
47 Kersten, D. Haberthür, and W. F. Kuhs (2015), Stop-and-go in situ tomography of dynamic
48 processes - gas hydrate formation in sedimentary matrices, *Acta Crystallographica Section A*,
49 71(a1), s154.

50

- 1 Gerner, A., Saenger, E. H., Shapiro, S. A. (2007), Attenuation of P-waves due to interlayer
2 fluid flow in hydrate-bearing sediments, *J. Geophys. Eng.*, 4(4), 394-403.
3
- 4 Gurevich, B., D. Makarynska, O. B. de Paula, and M. Pervukhina (2010), A simple model for
5 squirt-flow dispersion and attenuation in fluid-saturated granular rocks, *Geophysics*, 75, N109-
6 N120, doi: 10.1190/1.3509782.
- 7 Helgerud, M. B., Waite, W. F., Kirby, S. H., and Nur, A. (2003), Measured temperature and
8 pressure dependence of vp and vs in compacted, polycrystalline si methane and sii methane-
9 ethane hydrate., *Can. J. Phys.*, 81, 47–53.
10
- 11 Hu, G. W., Y. G. Ye, J. Zhang, C. L. Liu, S. B. Diao, and J. S. Wang (2010), Acoustic properties
12 of gas hydrate-bearing consolidated sediments and experimental testing of elastic velocity
13 models, *J. Geophys. Res.-Solid Earth*, 115, 11.
14
- 15 Jaeger, J. C., N. G. W. Cook, and R. W. Zimmerman (2007), *Fundamentals of rock mechanics*,
16 4th ed., Blackwell Publishing.
17
- 18 Kvenvolden, K. A. (1993), Gas hydrates - geological perspective and global change *Rev.*
19 *Geophys.*, 31, 173.
20
- 21 Li, F. G., C. Y. Sun, Q. Zhang, X. X. Liu, X. Q. Guo, and G. J. Chen (2011), Laboratory
22 Measurements of the Effects of Methane/Tetrahydrofuran Concentration and Grain Size on the
23 P-Wave Velocity of Hydrate-Bearing Sand, *Energy Fuels*, 25(5), 2076-2082.
24
- 25 [Liang, S., and P. G. Kusalik \(2011\), The mobility of water molecules through gas hydrates. *J.*](#)
26 [Am. Chem. Soc.](#), 133(6), 1870–1876, Doi: 10.1021/ja108434h.
- 27
- 28 Marín-Moreno, H., Sahoo, S. K.; Best, A. I. (2017), Theoretical modeling insights into elastic
29 wave attenuation mechanisms in marine sediments with pore-filling methane hydrate, *J.*
30 *Geophys. Res. Solid Earth*, 60(5).
31
- 32 Marone, F., and M. Stampanoni (2012), Regridding reconstruction algorithm for real-time
33 tomographic imaging, *Journal of Synchrotron Radiation*, 19(6), 1029-1037.
34
- 35 Mavko, G., and D. Jizba (1991), Estimating grain-scale fluid effects on velocity dispersion in
36 rocks, *Geophysics*, 56, 1940-1949, doi: 10.1190/1.1443005.
- 37 Müller, T. M., B. Gurevich, M. Lebedev (2010), Seismic wave attenuation and dispersion
38 resulting from wave-induced flow in porous rocks – A review. *Geophysics*, 75, 75A147–
39 75A164, doi: 10.1190/1.3463417.
- 40 Murphy, W. F., K. W. Winkler, and R. L. Kleinberg (1986), Acoustic relaxation in sedimentary
41 rocks, dependence on grain contacts and fluid saturation, *Geophysics*, 51, 757–766, doi:
42 10.1190/1.1442128.
- 43 Nixon, M. F. a. Grozic, J.L. (2007), Submarine slope failure due to gas hydrate dissociation: a
44 preliminary quantification, *Canadian Geotechnical Journal*, 44(3), 314 - 325.
45

1 O'Connell, R. J., and B. Budiansky (1977), Viscoelastic properties of fluid-saturated cracked
2 solids, *Journal of Geophysical Research – Solid Earth*, 82, 5719-5735, doi:
3 10.1029/JB082i036p05719.

4 Pimienta, L., J. Fortin, and Y. Guéguen (2015), Bulk modulus dispersion and attenuation in
5 sandstones, *Geophysics*, 80(2), D111-D127, doi: 10.1190/geo2014-0335.1.

6 Priest, J. A., A. I. Best, and C. R. I. Clayton (2006), Attenuation of seismic waves in methane
7 gas hydrate-bearing sand, *Geophys. J. Int.*, 164(1), 149-159.
8

9 Priest, J. A., E. V. L. Rees, and C. R. I. Clayton (2009), Influence of gas hydrate morphology
10 on the seismic velocities of sands, *J. Geophys. Res.-Solid Earth*, 114, 13.
11

12 Quintal, B., R. Jänicke, J. G. Rubino, H. Steeb, and K. Holliger (2014), Sensitivity of S-wave
13 attenuation to the connectivity of fractures in fluid-saturated rocks, *Geophysics*, 79, WB15-
14 WB24, doi: 10.1190/geo2013-0409.1.

15 Quintal, B., J. G. Rubino, E. Caspari, and K. Holliger (2016), A simple hydromechanical
16 approach for simulating squirt-type flow, *Geophysics*, 81, D335–D344, doi: 10.1190/geo2015-
17 0383.1.

18 Sams, M. S., J. P. Neep, M. H. Worthington, and M. S. King (1997), The measurement of
19 velocity dispersion and frequency-dependent intrinsic attenuation in sedimentary rocks,
20 *Geophysics*, 62(5), 1456-1464, doi: 10.1190/1.1444249.

21 Schicks, J. M., Spangenberg, E.; Giese, R.; Steinhauer, B.; Klump, J.; Luzi, M. (2011), New
22 Approaches for the Production of Hydrocarbons from Hydrate Bearing Sediments, *Energies*,
23 4(12), 151-172.
24

25 Schicks, J. S., Erik; Giese, R.; Luzi-Helbing, M.; Priegnitz, M.; Beeskow-Strauch, B. (2013),
26 A Counter-Current Heat-Exchange Reactor for the Thermal Stimulation of Hydrate-Bearing
27 Sediments, *Energies*, 6(6), 3002-3016.
28

29 Sell, K., Saenger, E.H., Falenty, A., Chaouachi, M., Haberthür, D., Enzmann, F., Kuhs, W.F.,
30 Kersten, M. (2016), On the path to the digital rock physics of gas hydrate-bearing sediments –
31 processing of in situ synchrotron-tomography data, 7, p. 1243-1258,
32

33 Sloan, E. D., and C. A. Koh (2008), *Clathrate hydrates of natural gases*, Third edition, CRC
34 Press, Boca Raton, USA.
35

36 Spangenberg, E., and Kulenkampff, J. (2006), Influence of methane hydrate content on
37 electrical sediment properties, *Geophys. Res. Lett.*, 33(24), 5.
38

39 Spangenberg, E. P., M.; Heeschen, K.; Schicks, J. M. (2015), Are Laboratory-Formed Hydrate-
40 Bearing Systems Analogous to Those in Nature?, *J. Chem. Eng. Data* 60(2), 258-268.
41

42 Subramanian, S., B. Quintal, C. Madonna, and E. H. Saenger (2015), Laboratory-based
43 seismic attenuation in Fontainebleau sandstone: Evidence of squirt flow, *Journal of*
44 *Geophysical Research – Solid Earth*, 120, 7526-7535, doi: 10.1002/2015JB012290.

- 1 Tisato, N., and B. Quintal (2013), Measurements of seismic attenuation and transient fluid
2 pressure in partially saturated Berea sandstone: evidence of fluid flow on the mesoscopic scale:
3 *Geophysical Journal International*, 195(1), 342-351, doi: 10.1093/gji/ggt259.
- 4 Tisato, N., and B. Quintal (2014), Laboratory measurements of seismic attenuation in
5 sandstone: Strain versus fluid saturation effects, *Geophysics*, 79, WB9-WB14, doi:
6 10.1190/geo2013-0419.1.
- 7 Tohidi, B., R. Anderson, M. B. Clennell, R. W. Burgass, and A. B. Biderkab (2001) Visual
8 observation of gas-hydrate formation and dissociation in synthetic porous media by means of
9 glass micromodels. *Geology*, 29(9), 867–870, Doi: 10.1130/0091-7613(2001).
- 10 Waite, W. F., et al. (2009), Physical properties of hydrate-bearing sediments, *Rev. Geophys.*,
11 47, 38.
12
- 13 White, J. E., 1975, Computed seismic speeds and attenuation in rocks with partial gas
14 saturation: *Geophysics*, 40, 224-232, doi: 10.1190/1.1440520.
- 15 White, J. E., N. G. Mikhaylova, and F. M. Lyakhovitskiy, 1975, Low-frequency seismic waves
16 in fluid-saturated layered rocks: *Izvestiya, Academy of Sciences, USSR. Physics of the Solid*
17 *Earth*, 11, 654-659.
- 18 Winkler, K. W., and A. Nur (1982). Seismic attenuation: Effects of pore fluids and frictional-
19 sliding. *Geophysics*, 47, 1-15, doi: 10.1190/1.1441276.
- 20
- 21 Yun, T. S., F. M. Francisca, J. C. Santamarina, and C. Ruppel (2005), Compressional and shear
22 wave velocities in uncemented sediment containing gas hydrate, *Geophys. Res. Lett.*, 32(10),
23 5.
24
- 25 Zhang, Q., F. G. Li, C. Y. Sun, Q. P. Li, X. Y. Wu, B. Liu, and G. J. Chen (2011),
26 Compressional wave velocity measurements through sandy sediments containing methane
27 hydrate, *Am. Miner.*, 96(10), 1425-1432.
28